



PCCP

The Benefit of Poor Mixing: Kinetics of Coacervation

Journal:	<i>Physical Chemistry Chemical Physics</i>
Manuscript ID	CP-ART-06-2020-003224.R1
Article Type:	Paper
Date Submitted by the Author:	26-Aug-2020
Complete List of Authors:	Blocher McTigue, Whitney; University of Massachusetts Amherst, Department of Chemical Engineering Voke, Elizabeth; University of Massachusetts Amherst, Department of Chemical Engineering Chang, Li-Wei; University of Massachusetts Amherst, Department of Chemical Engineering Perry, Sarah; University of Massachusetts Amherst, Department of Chemical Engineering

SCHOLARONE™
Manuscripts

The Benefit of Poor Mixing: Kinetics of Coacervation

Whitney C. Blocher McTigue, Elizabeth Voke, Li-Wei Chang, and Sarah L. Perry*

Department of Chemical Engineering, University of Massachusetts Amherst

*Correspondence: perrys@engin.umass.edu

Abstract:

Complex coacervation has become a prominent area of research in the fields of food science, personal care, drug stabilization, and more. However, little has been reported on the kinetics of assembly of coacervation itself. Here, we describe a simple, low-cost way of looking at the kinetics of coacervation by creating poorly mixed samples. In particular, we examine how polymer chain length, the patterning and symmetry of charges on the oppositely charged polyelectrolytes, and the presence of salt and a zwitterionic buffer affect the kinetics of complex coacervation. Our results suggest an interesting relationship between the time for equilibration and the order of addition of polymers with asymmetric patterns of charge. Furthermore, we demonstrated that increasing polymer chain length resulted in a non-monotonic trend in the sample equilibration times as a result of opposing factors such as excluded volume and diffusion. We also observed differences in the rate of sample equilibration based on the presence of a neutral, zwitterionic buffer, as well as the presence and identity of added salt, consistent with previous reports of salt-specific effects on the rheology of complex coacervates. While not a replacement for more advanced characterization strategies, this turbidity-based method could serve as a screening tool to identify interesting and unique phenomena for further study.

Introduction:

Complex coacervation is an associative, liquid-liquid phase separation phenomenon driven by an initial electrostatic attraction between oppositely charged macroions.¹⁻⁷ This attraction is followed by entropic gains from the release of small, bound counter-ions and the restructuring of water molecules.⁸⁻¹¹ Phase separation typically results in the formation of coacervates as a dispersion of macromolecule-rich (*e.g.*, polymer, protein, etc.) droplets in equilibrium with a macromolecule-poor phase, called the supernatant.^{8,9,12-21} The scope of coacervation has expanded from its original focus on proteins and polysaccharides²²⁻²⁴ and their applications in food to include polynucleotides,²⁵⁻³⁰ synthetic polymers,³¹⁻³⁷ surfactants,³⁸⁻⁴⁵ nanoparticles,^{46,47} and other hierarchical assemblies⁴⁸⁻⁵⁵ and its use has extended into fields such as adhesives,⁵⁶⁻⁷¹ drug delivery,^{2,12,15,25,27,28,32,34,72-88} nano/bio-reactors,^{31,33,89-91} and cellular biology.^{25,92-109}

Much of the utility of coacervates has come from their ability to effectively encapsulate cargo and/or respond to their environment. Therefore, the vast majority of studies on coacervate materials require mapping out some aspect of the phase behavior of these materials. While a number of recent reports have quantitatively mapped out the entire two-phase region,¹¹⁰⁻¹¹⁴ most studies take advantage of turbidity or light scattering to simply determine conditions where coacervates form.^{8,14,17,115-118} These characterizations of phase behavior can often be accelerated through the use of automation, particularly by helping decrease the required sample volumes. This need for small sample volumes is particularly acute in many biologically-inspired or bio-relevant systems where it can be challenging to obtain large quantities of material.

In contrast to the number of studies aimed at characterizing the thermodynamic phase behavior of complex coacervation, there are significantly fewer efforts that look into the dynamic nature of coacervate formation. There are kinetic studies dedicated to the formation of polyelectrolyte complexes broadly,¹¹⁹⁻¹²⁵ as well as on liquid complex coacervation specifically.^{46,80,126-128} The majority of studies take advantage of techniques such as turbidity,⁴⁶ light scattering,^{122,123,127} or small angle X-ray scattering¹¹⁹ to track coacervate evolution. These studies tend to take advantage of fast mixing, such that the kinetics of complexation can be monitored after both polyelectrolytes have come into contact with each other.^{46,119,121-124,127} Much of this work focuses on the nucleation and early-time evolution of complexes in dilute solution, looking at parameters such as salt, pH, and mixing/charge ratio.^{46,119,121-124,127} However, the evolution of coacervate materials in formulations relevant for real-world applications can be very different than what is observed in well-mixed laboratory samples. Here, complicating factors such as differences in the concentration of the various components and/or the order of component addition^{126,127,129} can have a significant effect on the resulting product and/or the time needed for it to equilibrate. While such formulation questions can be answered via large-scale direct experiments, we discuss a method that takes advantage of the types of turbidity experiments that researchers are already performing to answer these questions at a much smaller scale.

Here, we describe a simple, method for studying the kinetics of coacervate formulation by tracking the time evolution of the turbidity of dilute, poorly mixed coacervating samples prepared at a range of polycation/polyanion ratios. We examine the kinetics of coacervation for polypeptides with a range of chain lengths and sequences. We also study how the addition of salt, the identity of the salts, and the presence of a zwitterionic buffer affects the kinetics of complexation and the sensitivity of these parameters to the order of polymer addition to the sample.

Materials and Methods:

Materials:

Abbreviations for reagents are as follows: tert-butoxycarbonyl (Boc); 9-fluorenylmethoxycarbonyl (Fmoc); t-butyl (tBu); trifluoroacetic acid (TFA); triisopropylsilane (TIPS); N,N-dimethylformamide (DMF); dichloromethane (DCM); N,N-diisopropylcarbodiimide (DIC); lysine (Lys or K); glutamate (Glu or E); glycine (Gly or G); ethyl (hydroxyimino)cyanoacetate (Oxyma); 4-(2-hydroxyethyl)-1-piperazineethanesulfonic acid (HEPES).

Sequencing grade DMF, GC/MS grade DCM, TFA, ethyl ether anhydrous (BHT stabilized), methanol and acetonitrile (HPLC grade) were purchased from Fisher Scientific. Piperidine, α -cyano-4-hydroxycinnamic acid, isopropanol (99%) was purchased from Sigma Aldrich. DIC (99%), TIPS (98%) was purchased from Acros Organics. Rink amide MBHA resin (loading level 0.32 mmol/g), Fmoc-*L*-Lys(Boc)-OH, Fmoc-*D*-Lys(Boc)-OH, Fmoc-*L*-Glu(tBu)-OH, Fmoc-*D*-Glu(tBu)-OH, Fmoc-Gly-OH, and Oxyma were all purchased from Peptide Solutions, LLC. All water was dispensed from a Milli-Q water purification system at a resistivity of 18.2 M Ω .cm (Millipore).

Zwitterionic HEPES buffer ($\geq 99\%$) was purchased as a powder from Fisher Scientific and made into a 0.5 M stock solution adjusted to pH 7.0. Sodium chloride, potassium chloride, and sodium bromide were purchased as powders from Sigma Aldrich. Potassium bromide was purchased from Fisher Scientific as a powder. All salt stocks were made at 0.5 M and adjusted to pH 7.0.

Peptide Synthesis:

Polypeptides with N = 50 were prepared using standard Fmoc-based solid-phase synthesis on a Liberty Blue automated microwave peptide synthesizer from CEM, Ltd.¹³⁰ Deprotection and coupling were performed under microwave irradiation on a Rink amide MBHA resin with 0.2 M Fmoc and Boc protected lysine (Fmoc-*L*-Lys(Boc)-OH, Fmoc-*D*-Lys(Boc)-OH), Fmoc and tBu protected glutamate (Fmoc-*L*-Glu(tBu)-OH, Fmoc-*D*-Glu(tBu)-OH), and Fmoc protected glycine (Fmoc-Gly-OH) in DMF. 20% Piperidine in DMF was used for Fmoc deprotection. DIC and Oxyma in a 0.5 M and 1.0 M concentration in DMF were used as activator and base, respectively.

Cleavage from the resin and side-chain deprotection was performed using 10 mL of TFA/water/TIPS in the volume ratio of 95/2.5/2.5 for 3 hours at room temperature while bubbling with carbon dioxide. The cleaved product and resin were separated by filtration. The crude peptide was then precipitated into 40 mL of cold (stored at -80°C) anhydrous ethyl ether. The mixture was then centrifuged for 5 min at 5,000 rpm (Sorvall Legend X1R Centrifuge, Thermo Fisher Scientific, Inc.). The supernatant was decanted and a second round of precipitation and centrifugation was performed. The crude product was then dried *in vacuo* in a desiccator overnight. All glutamate polymers were pH balanced after synthesis for solubility and then lyophilized.

Characterization of the final product was performed via a Bruker UltrafleXtreme (Fremont, CA, USA) matrix-assisted laser desorption/ionization time of flight mass spectrometer (MALDI-TOF). Samples of the peptide were mixed with matrix solution (approximately 50 mg/mL α -cyano-4-hydroxycinnamic acid dissolved in 1:1 mixture of water and acetonitrile with 0.05%

TFA) in 1:1 ratio to reach a final concentration of approximately 7.5 mM peptide.

Poly(glutamate) with degree of polymerization $N = 50$ was synthesized using amino acids of alternating chirality (D and L) to mitigate inter-peptide hydrogen bond formation,^{10,13,131,132} while poly(lysine) with $N = 50$ was synthesized only using amino acids of L chirality. Sequence-defined poly(lysine-*co*-glycine) (K_xG_y) _{N} and poly(glutamate-*co*-glycine) (E_xG_y) _{N} peptides were synthesized with a degree of polymerization $N = 50$. Thus, all peptides include the charge-patterned blocks of 48 amino acids described by the block size, and are capped on each terminus by a single amino acid (K, E, or G, Table 1). For a block size of 16, the lysine or glutamate portions of the peptide were synthesized using amino acids of alternating chirality (D and L) to mitigate inter-peptide hydrogen bond formation.^{10,13,131,132} This use of alternating chirality was only implemented for the longest block size because of the tendency for complexing peptides to form β -sheets when a continuous run of more than 7-8 chiral amino acids is present.^{10,132} Lysine residues exist as TFA salts, while glutamate residues are present as sodium salts.

Table 1. Molecular sequence for poly(lysine-*co*-glycine) or poly(glutamate-*co*-glycine), denoting lysine or glutamate with an X, peptides with degree of polymerization $N = 50$.

Block Size	Polypeptide Sequence
2	(XG) ₂₅
4	G(XXGG) ₁₂ X
8	G(X ₄ G ₄) ₆ X
16	G(X ₈ G ₈) ₃ X

Poly(L -lysine trifluoroacetate or bromide) and poly(D,L -glutamate sodium salt) with chain lengths of $N = 100, 400,$ and 800 were purchased from Alamanda Polymers and used without further purification. These polymers were synthesized via N-carboxyanhydride polymerization using an alkylamine initiator.¹³³ The degree of polymerization was reported by the manufacturer based on ¹H NMR analysis with a polydispersity index (PDI) between 1.01 and 1.08 for all $N = 100, 400,$ and 800 polymers (Table S2). Table S2 also includes mean squared radius of gyration estimations assuming ideal flexible chain behavior.

Coacervate Preparation:

Polypeptide stock solutions were prepared gravimetrically using Milli-Q water at a concentration based on the total number of amino acids present. For instance, a stock solution of poly(glutamate) of 10 mM amino acid would be used in parallel with a stock solution of the poly(lysine-*co*-glycine), also at 10 mM with respect to the total number of amino acids, or 5 mM with respect to the number of charged monomers present in solution. All solutions were adjusted to $\text{pH} = 7.0 \pm 0.03$ using concentrated solutions of HCl and NaOH, as needed. Monomer concentration was chosen as the experimental basis in order to easily enable direct stoichiometric comparison of the number of positively and negatively charged units present in solution.

Complexation was achieved by mixing aqueous solutions of cationic poly(lysine)-based peptides with anionic poly(glutamate)-based peptides, potentially in the presence of buffer and/or additional salt. Samples were prepared using a Biomek NX^P (Beckman Coulter) liquid handling

robot. Water, followed by concentrated solutions of buffer and salt, as needed, were pipetted into a Falcon flat bottom 384-well plate (Fisher Scientific). The first polypeptide was added and the solution was then mixed using an orbital shaker for 15 s, after which the second polypeptide was added to a final sample volume of 35 μL per well. The final sample was mixed again for 30 s using the orbital shaker. All samples were prepared in triplicate.

For experiments intended to investigate the kinetics of coacervate assembly, the small volume and rounded square shape of the wells in a 384-well plate did not allow for effective mixing, allowing us to monitor the samples as they reach equilibrium. However, preparation of samples in a larger volume, such as a 96-well plate with a total sample volume of 150 μL per well, did allow for fast mixing and samples could be moved from the 96-well plate to the 384-well plate fully equilibrated.

Complexation was performed over a range of different ratios of positive and negatively charged polypeptides at a total monomer concentration of 2 mM, at pH 7.0. Under these conditions, it is a reasonable approximation to describe both lysine and glutamate as fully charged. Two experiments were run simultaneously to test the order of the addition for the polypeptides; one where the polyanion was pipetted into the well plate first and another where the polycation was added first. Each experiment was performed at sixteen different charge fractions, although the selection of data points to be sampled was skewed in favor of net negative or net positive conditions, based on the order of peptide addition. Immediately following sample preparation, the well plate was transferred to the plate reader for analysis.

Two control experiments were performed to establish how mixing affects our experimental results. The first, well-mixed experiment was prepared by hand, at a total sample volume of 120 μL per tube, using $(\text{EG})_{25}/(\text{KG})_{25}$ where the same procedure as described above was followed, pipetting solutions into 1.5 mL Eppendorf tubes and vortexing for approximately 5 s after the addition of each solution. Three 35 μL aliquots were then transferred to a 384-well plate for each sample. The plate was read immediately after making the samples and pipetting them into the plate. The goal of the second control experiment was to test the effect of the orbital shaker on the Biomek liquid handling robot. This experiment used same system of $(\text{EG})_{25}/(\text{KG})_{25}$, and samples were prepared using the Biomek. The same procedure was used, but the mixing steps were removed.

Turbidity Analysis:

A plate reader equipped with a UV spectrophotometer (Synergy H1, BioTek, Inc.) was used to measure changes in the turbidity at a wavelength of 562 nm as a function of time. None of the polymers absorb light at this wavelength; thus, turbidity is due to light scattering from suspended coacervate droplets. Turbidity is defined by $-\ln(I/I_0)$, with I_0 = incident light intensity and I = intensity of light passed through the sample volume.

Static turbidity measurements were used for characterization of well-mixed samples, followed by examination of samples via optical microscopy (EVOS XL Core, Fisher Scientific) to confirm coacervate formation. These samples were imaged directly after preparation.

For time-resolved experiments, turbidity data were collected every 5 min for 90 min, unless otherwise noted. For the control experiment, where no plate mixing steps were performed during

sample preparation, turbidity measurements were taken every 5 min for 6 h.

Data Analysis:

MATLAB (The Mathworks Inc.) scripts were written to fit a Gaussian unimodal curve to describe the stoichiometric curve at each time point. These curves were then used to track shifts in the observed phase behavior as a function of time. The Gaussian is described as:

$$G = Ae^{-\frac{(x-b)^2}{2c^2}} \quad (1)$$

A is the height of the peak, b is the position of the center of the peak, c is the standard deviation of the curve, and x is the independent variable, which is the charge fraction. The code found the maximum turbidity, the position of this maximum, and the standard deviation of the all the turbidities at each time point and used these as initial guesses for A , b , and c , respectively. The built-in MATLAB function *nlinfit* was then utilized to find the best parameters for each Gaussian time set. The full MATLAB code is available in the Supplementary Information.

Using the peak locations from the Gaussian models, a peak location versus time curve was constructed along with confidence intervals for the peak location based on the variation in the raw data. We defined the time to reach equilibrium as the time point at which the peak location first reached its maximum or minimum, depending on the order of addition. In addition to this elapsed time calculation, we also evaluated our data by determining the “half-time,” or the time required to reach half of the maximum or minimum value. Details on this method are described in the Supplementary Information and all elapsed times and half-times are outlined in Table S1.

Results and Discussion:

The goal of these experiments was to understand the formation and equilibration aspects of complex coacervates using small volumes of material. This approach has the benefit of being accessible to a wide range of scientists, and also has the potential to provide insight into the formulation requirements of coacervate materials.

Coacervation by Hand and by Machine:

When two oppositely charged polyelectrolytes are brought together to form a complex coacervate, maximum complex formation is typically observed under conditions of charge neutrality. Thus, if the two polyelectrolytes are of equal length and charge density, net neutrality and the maximum level of complexation is expected to occur with equal numbers of each polyelectrolyte. These trends as a function of the charge stoichiometry of the system are easily observed through the use of turbidimetry. Samples for such experiments are typically prepared using a pipette, microcentrifuge tubes, and a vortex mixer, and a key aspect of any protocol is ensuring that the samples are fully equilibrated. The equilibrium nature of complex coacervation is often determined by testing whether or not changing the order of addition of the components affects the results.^{21,131,134,135} An example of results from a well-mixed, fully-equilibrated turbidity experiment for the oppositely-charged polypeptides of poly(lysine-*co*-glycine) and poly(glutamate-*co*-glycine) is shown in Figure 1 (black curve), and previous reports of polypeptide-based complex coacervation, as well as our own experience, have suggested that the hydrophilic nature of these peptide-based materials allows for easy sample preparation and

equilibration.^{6,8,10,13,16,17,20,48,131,135-137}

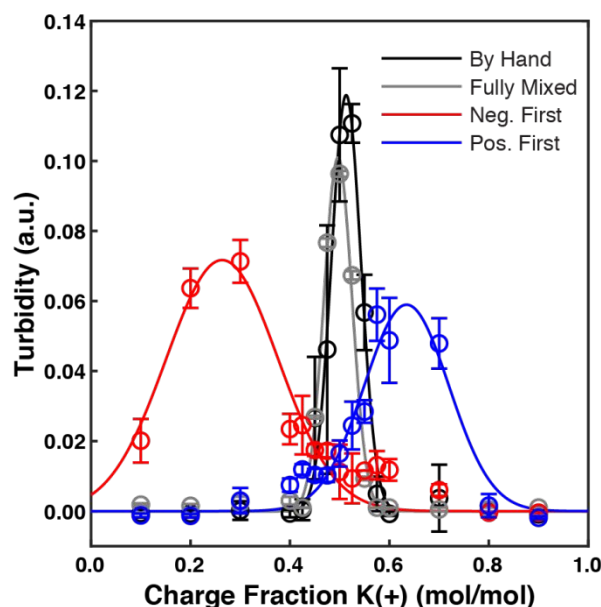


Figure 1. Stoichiometry experiment showing turbidity as a function of the mole fraction of cationic monomer present for coacervates of $(EG)_{25}/(KG)_{25}$ prepared “by hand” pipetting and vortexing (black), as “fully mixed” samples prepared by the liquid handling robot using a 96-well plate, followed by aliquoting into a 384-well plate for analysis (grey), and poorly mixed samples prepared by the liquid handling robot directly into a 384-well plate named “Neg. First” with the negative polyelectrolyte added first (red) or “Pos. First” with the positive polyelectrolyte added first (blue). Error bars represent the standard deviation of $N = 27$.

While the preparation of samples by hand allows for excellent control over sample mixing, the need to survey a broad range of formulation conditions often calls for scaling down and automation of the experiments. To this end, we decreased the scale of our experiments from a total volume of 120 μL prepared by hand in a single microcentrifuge tube and aliquoted into a 384-well plate, to direct preparation of 35 μL -scale samples in the well plate using a liquid handling robot. However, we were surprised to discover that the results from a standard stoichiometry experiment did not match those that we regularly obtained by hand. Rather than observing a peak at the charge-neutral mole fraction of 0.5, our maximum was shifted to lower cationic charge fractions (Figure 1, red curve).

Our standard protocol for preparing coacervate samples involved the mixing of water, followed by buffer/salt (as needed), and then the polyanion followed by the polycation. However, given the surprising result that we had obtained with our first experiment, we then ran a test with the polycation added first. Interestingly, whereas the experiment with the polyanion added first showed a peak in the turbidity at net negative mole fractions, our “polycation first” experiments showed a peak in the turbidity at net positive mole fractions (Figure 1, blue curve). Subsequent tests demonstrated that we could eliminate this phenomenon by preparing samples in a larger, 96-well plate, followed by aliquoting into the 384-well plate for analysis (Figure 1, grey curve).

The different turbidity results obtained from the direct preparation of samples into the small well (roughly 3 mm by 3 mm square) of a 384-well plate compared with those of a 96-well plate (~ 6.35 mm diameter circle) suggested that the size of the different wells might be directly

affecting the ability of the polymers to mix. Quick calculations using the well plate dimensions and an orbital mixing speed of 950 rpm allow us to estimate the Reynolds number (*i.e.*, the ratio of inertial to viscous forces) for water at 25°C in the 384-well plate as $Re \sim 546$, whereas for the larger 96-well plate $Re \sim 2,247$. These results suggest that flow in the 384-well plate is laminar (*i.e.*, $Re < 2,200$), while the 96-well plate experiences transitional flow (*i.e.*, $4,000 > Re > 2,200$). Furthermore, we estimated the timescale for purely diffusive mixing for the polymer to move halfway across the well as ~ 3.4 hr and ~ 14.0 hr for the 384- and 96-well plates, respectively. Thus, the enhancement of the more chaotic flow allows for better mixing in the 96-well plate versus the purely laminar flow in the 384-well plate. Details of the calculations are available in the Supplementary Information.

While we were able to develop protocols that allowed us to operate our liquid handling robot in a manner such that we could reproduce results obtained by hand, we were also interested in further exploring the observation that poor mixing could lead to differences in the observed outcome. To this end, we used the liquid handling robot to directly prepare “poorly mixed” samples in 384-well plates, and used a plate reader to track changes in the turbidity signal as a function of time. These first experiments involved sequence-controlled polypeptides that were symmetric to each other with respect to charge pattern; a polyanion with an alternating sequence of one neutral monomer and one negatively charged monomer would be paired with a polycation with the equivalent charge pattern (*i.e.*, $(EG)_{25}/(KG)_{25}$ using the single letter notation for amino acids). As in Figure 1, when the positively charged polypeptide was added first, the turbidity signal was first observed to the right of net neutrality, at “net positive” conditions. Over the course of 90 minutes, the turbidity signal shifted back to equilibrate around net neutral conditions (Figure 2a). The opposite trend was observed when the polyanion was added first, showing an initial turbidity signal at “net negative” conditions that shifted up to net neutrality (Figure 2c). It is interesting to note that the symmetry in the structure and charge density of the peptides is matched by the symmetry in timescales for equilibration. Similarly symmetric results were seen for matched pairs of polypeptides including homopolymers (Figures S1 and S2) and those with different charge block sizes (Figures S3 and S4), suggesting that this is a general phenomenon.

We determined a characteristic time for equilibration by first fitting the raw turbidity data at each time point using a Gaussian peak. This peak location data could then be plotted as a function of time (Figure 2b,d). We then chose to characterize the equilibration time for our system as the time at which the turbidity signal first reached its final peak location (*i.e.*, elapsed time, Figure 2b,d black squares). It was also possible to determine a characteristic half-time for equilibration (Figure 2b,d black diamonds). However, the time needed to transport the samples between the liquid handling robot and the plate reader made collection of data at very short timescales difficult. Thus, while similar trends were observed when using half-times, we have elected to utilize the “elapsed” timescale as our characteristic measure. We also note that there was a slight difference in the preparation and readout timescale between samples where the negative polyelectrolyte added first and the positive polyelectrolyte added first due to the sequential way in which the samples were prepared and the turbidity was read. Both directions were done together in one experiment, with samples where the polyanion was added first prepared and measured before those where the polycation was added first. We estimate that this difference is less than 1 min. To account for this, the average between the two times were used.

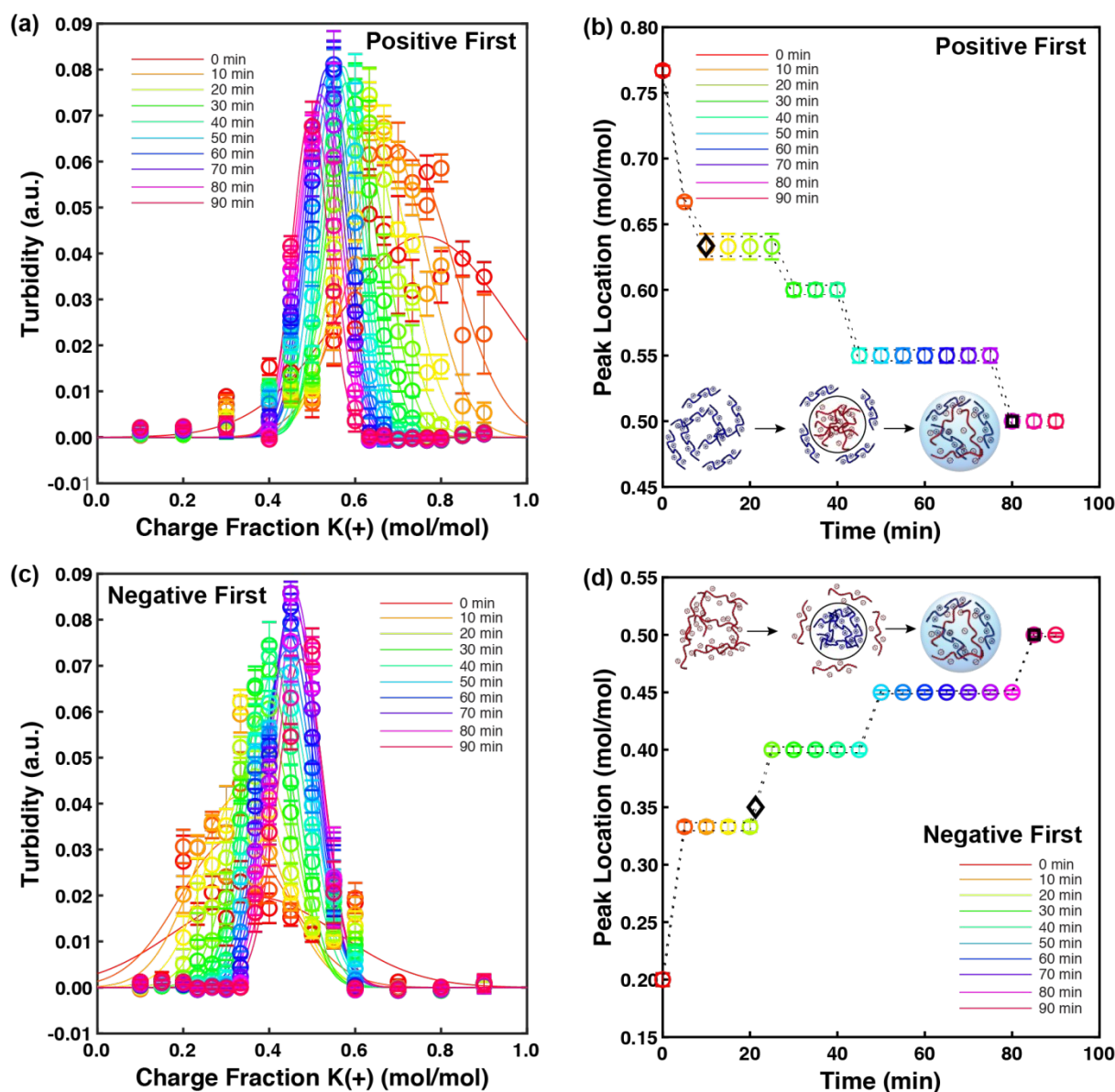


Figure 2. Plots of the evolution of turbidity as a function of the cationic charge fraction and time for the complexation of (EG)₂₅/(KG)₂₅ at pH 7.0 in water for samples where the (a) concentrated (EG)₂₅ was mixed into dilute (KG)₂₅, (“positive first”) and the opposite case (c) where the concentrated (KG)₂₅ was added into dilute (EG)₂₅ (“negative first”). Plots of peak location versus time for (b) (KG)₂₅ added first and (d) (EG)₂₅ added first. Schematic representations of the mixing conditions are shown in (b) and (d). Black symbols indicate the characteristic times for sample equilibration, with diamonds marking the half times and black squares marking the elapsed time. Elapsed times for (a) and (b) are 80 min and 85 min, respectively. Error bars represent the standard deviation of N = 27.

Exploring the Effect of Sequence in the Presence of Buffer:

Inspired by the results shown in Figure 2, we decided to expand our study to include a broader set of peptides. We also decided to buffer our system with a zwitterionic (net neutral) buffer, HEPES, to better maintain a constant pH of 7.0. Initial experiments had demonstrated that the addition of 10 mM HEPES did not have a significant effect on the turbidity signal observed during a stoichiometry experiment, and only a small effect on the phase behavior of our coacervates, reducing the salt resistance of the resulting coacervate slightly, but less than the

addition of an equivalent concentration of another salt (see Figure S5).

Symmetry in Polypeptides:

To begin with, we repeated the experiment with $(EG)_{25}/(KG)_{25}$ shown in Figure 2, this time with the addition of buffer. Interestingly, we observed that the addition of 10 mM HEPES as a neutral, zwitterionic buffer resulted in a smaller offset for the initial turbidity signal from net neutrality (Figure 3). While the trends are the same for both directions, the first peak in the positive first data at $t = 0$ without buffer was observed at 0.760, while the one with buffer occurred at 0.530. Similarly, for the negative first experiment the first peak without buffer was observed at 0.367 while the one with buffer occurred at 0.415. In addition to and consistent with a decrease in the observed initial offset in our turbidity data, the addition of buffer also served to accelerate the overall time for equilibration. In the absence of buffer, the average elapsed time for equilibration was 82.5 min, whereas with buffer it decreased to 50.0 min. This dramatic acceleration (a roughly ~40% decrease in elapsed time) was unexpected given the fact that the ~86% of the salt resistance was retained with the addition of 10 mM of HEPES buffer. Further studies looking into the rheological effects of small molecules such as the zwitterionic HEPES buffer would help to elucidate this trend, but are beyond the scope of the current work.

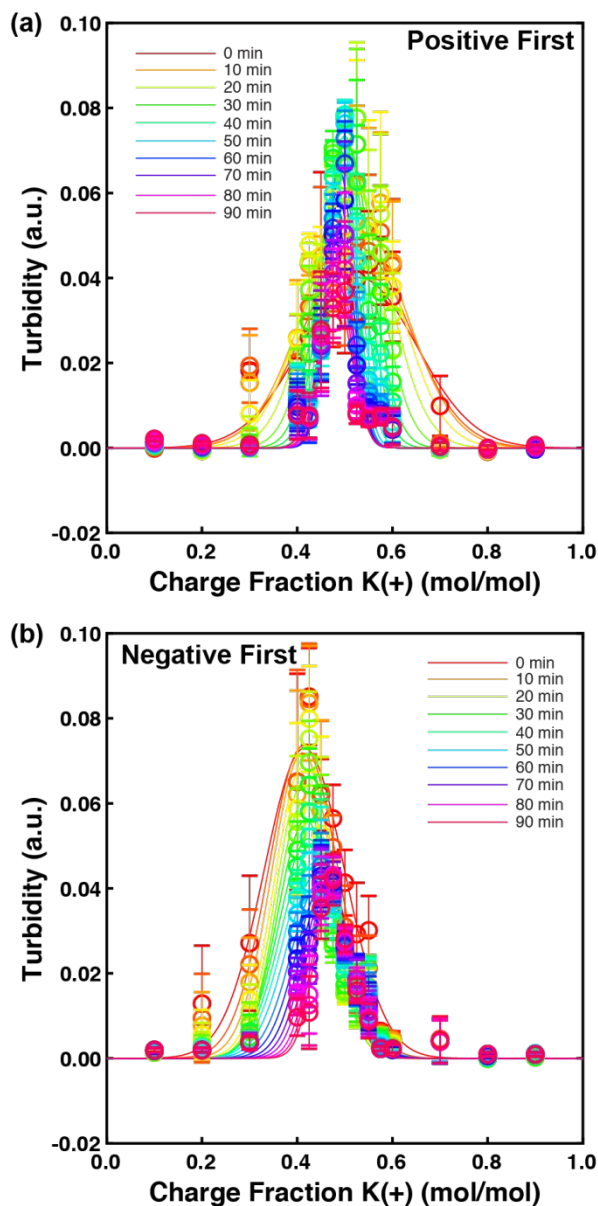


Figure 3. Plots of the evolution of turbidity as a function of the cationic charge fraction and time for the complexation of $(EG)_{25}/(KG)_{25}$ at pH 7.0 in water for samples where the (a) concentrated $(EG)_{25}$ was mixed into dilute $(KG)_{25}$, (“positive first”) and the opposite case (c) where the concentrated $(KG)_{25}$ was added into dilute $(EG)_{25}$ (“negative first”) in 10 mM HEPES buffer. The elapsed time for sample equilibration was determined to be 30 min for (a) and 70 min for (b). Error bars represent the standard deviation of $N = 27$.

Asymmetry in Polypeptides:

After investigating complexation between polypeptides with the same sequence and charge density, we then moved on to consider two polypeptides that were not symmetrical to each other. In particular, we substituted one of the peptides from our previous system with the fully-charged homopolymer (*i.e.*, $(KG)_{25}/E_{50}$ and $K_{50}/(EG)_{25}$).

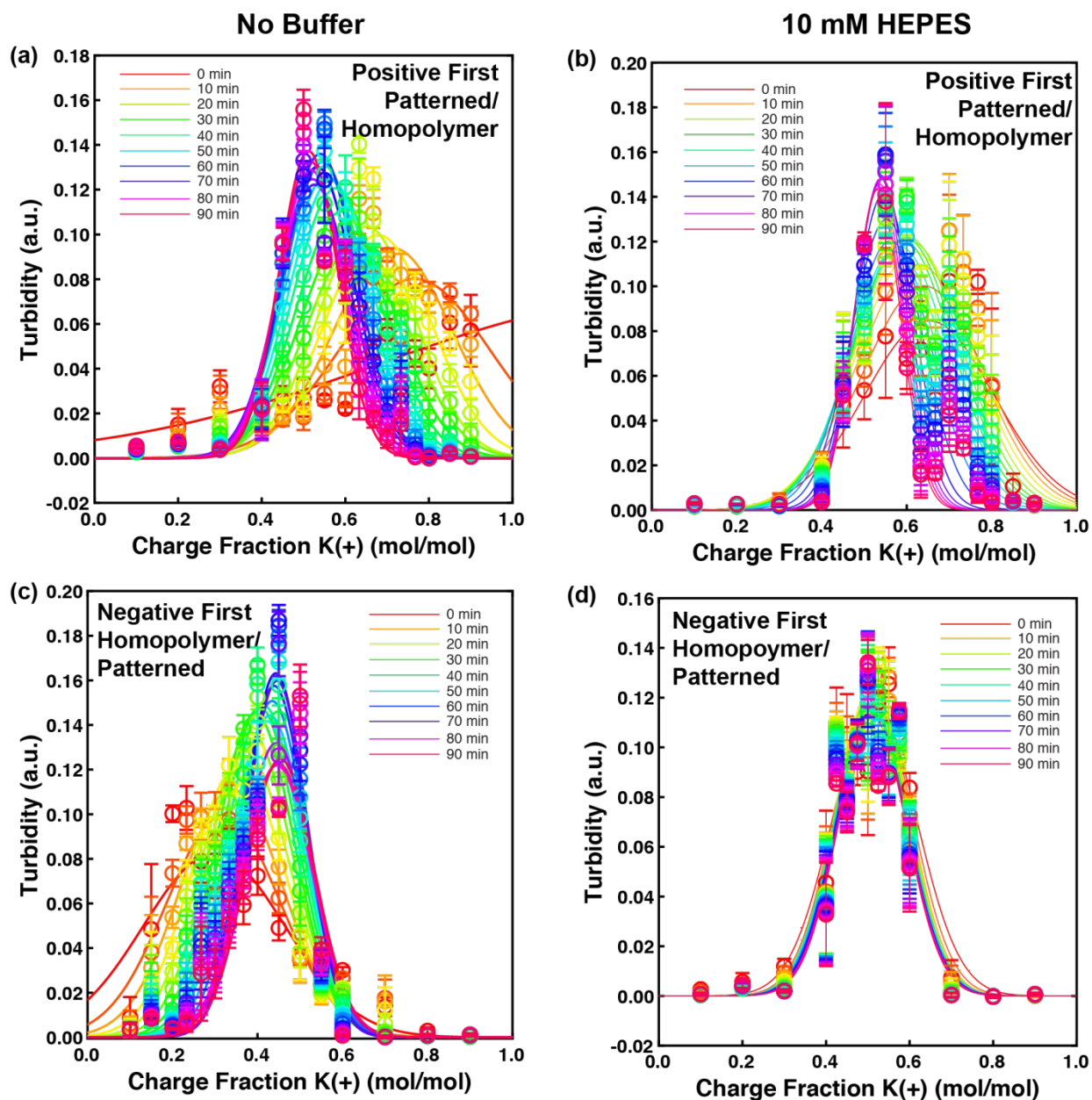


Figure 4. Plots of the evolution of turbidity as a function of the cationic charge fraction and time for the complexation of E_{50} and $(KG)_{25}$. **(a)** Shows the addition of $(KG)_{25}$ first and **(c)** shows the addition of E_{50} first. **(b)** Shows the addition of $(KG)_{25}$ first and **(d)** shows the addition of E_{50} first in the presence of 10 mM HEPES. When the patterned polyelectrolyte was added first in the presence of buffer, there is an initial offset followed by a shift toward equilibrium, whereas there is little to no offset observed when the homopolymer is added first. Elapsed time is **(a)** 65 min and **(c)** 75 min with no buffer and **(b)** 85 min and **(d)** 15 min in the presence of 10 mM HEPES. Error bars represent the standard deviation of $N = 27$.

Replacing a half-charged peptide with a fully-charged homopolymer of the same overall length represented the most drastic change that we could make in our materials while keeping chain length constant. While our previous results had shown relatively symmetric behavior with respect to the order of addition, for these mismatched, or asymmetric polypeptide systems we observed a significant difference in the equilibration behavior depending on which polymer was added first. In our pH buffered system, the addition of the patterned polypeptide first showed

results that were similar, though slightly faster, to those observed previously for the unbuffered system (Figure 4a,b). However, when the homopolymer was added first, the turbidity signal equilibrated to the expected conditions around net neutrality almost immediately when buffer was present (Figure 4d). Similar trends were observed for other peptide systems, regardless of the identity of the patterned/homopolypeptides (see Figure S6). However, in the absence of buffer, we do not see the almost instantaneous equilibration with the addition of the homopolymer added first (Figure 4c). These data suggest that presence or absence of even a zwitterionic buffer is a means by which the equilibration time can be tuned, and that this particular phenomenon may be very sensitive to the density of charges present on the polymers. Further exploration of this potential phenomenon, as well as a more in depth exploration of sequence on the rates of equilibration is an interesting area for future study. In particular, the dramatic effects of charge patterning mismatch could have significant implications when applied to industrial-scale formulation.

Is This Just Diffusion? Chain Length of Polypeptides:

An obvious question related to the varying results presented thus far is whether the observed differences are evidence of anything other than diffusion. For symmetric peptide systems, the molecular weights of the lysine and glutamate copolymers are similar, and thus symmetric trends in the data would not be unreasonable. Additionally, the addition of buffer seems to act like a salt, though to a lesser extent, because of its zwitterionic nature. However, our observations for asymmetric coacervate systems (Figures 4, S6-S8) suggest that forces beyond simple diffusion are at play.

To test whether or not the temporal changes in the turbidity results were caused by merely diffusion, we first examined the effect of polymer chain length. If diffusive effects were the dominant factor in our experimental observations, we would expect to observe an increase in the elapsed time for equilibration with increasing polypeptide chain length. We tested coacervation between K_N and E_N with degree of polymerization $N = 50, 100, 400, \text{ and } 800$. These experiments were performed in the absence of buffer so as to slow down the timescales for equilibration and allow for clear differentiation of the different polymer systems.

Our experimental results showed a non-monotonic dependence on chain length, with a maximum equilibration time observed with $N = 100$, followed by a subsequent decrease in the equilibration time with increasing chain length (Figure 5). Diffusivity is expected to scale as $\sim N^{-1}$.¹³⁸ However, in order to observe the “volcano” type of trend with increasing chain length, there must be another factor that accelerates motion with increasing chain length. While a detailed exploration of this phenomenon is beyond the scope of the current publication, we hypothesize that factors such as excluded volume effects analogous to those observed in size exclusion chromatography, exchange dynamics within a polyelectrolyte complex, as well as differences in the driving force for complexation may play a role. Thus, both the length and the charge density of the polymers appear to play a significant role in determining the timescale for a coacervating system to equilibrate.

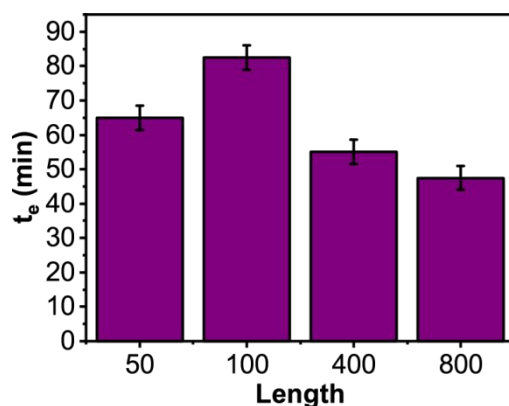


Figure 5. Average elapsed for the equilibration of K_N and E_N as a function of polypeptide lengths $N = 50, 100, 400,$ and 800 with no buffer present. Error bars represent the propagated error.

Effect of Salt:

The combination of results presented thus far suggested that the differences in equilibration time for our poorly mixed turbidimetry experiments could provide insight into the strength of interactions between polymer species in our coacervate materials, somewhat analogous to either a viscosity or a stress relaxation measurement. The addition of salt has long been used as a way of modulating the rheological properties of complex coacervates and polyelectrolyte complexes generally.^{113,137,139-144} Thus, we investigated the effect of added salt and salt identity on coacervate equilibration.

To begin with, we tested the effect of increasing salt concentration. In Figure 6a, we compare the elapsed time for complexation between $(EG)_{25}$ and $(KG)_{25}$ in the absence of added salt, as well as the addition of 10 mM and 25 mM KBr. The addition of even a small amount of salt has a tremendous effect on the time needed for sample equilibration, with the average elapsed time decreasing from 82.5 min to 5.0 min with the addition of only 10 mM KBr. With the addition of higher salt concentrations, the calculated elapsed time decreased further, and it became difficult to accurately determine a time scale.

Our results correlate with reports from the literature that salt accelerates both the kinetics of coacervate formation and the timescale for relaxation. Liu *et al.* used stopped-flow light scattering to study the kinetics of coacervation upon fast mixing of two oppositely-charged polymers.^{126,127} The time scale for complexation decreased with the increasing addition of salt, similar to trends found with our data.¹²⁷ A report by Salehi *et al.*, on the layer-by-layer assembly of polyelectrolytes, illustrated an optimum range of salt between 15-60% of the maximum salt concentration where complexation can occur where there is a faster growth.¹²¹ However, this report, and other reports, focused solely on one type of salt with different systems, making it difficult to draw conclusions of how the type of salt affects the kinetics.^{119,121} Further exploration and comparison of different salts could help elucidate the effects of salt composition on the kinetics of polyelectrolyte complexation. These parallel results with respect to salt are in contrast to the absence of reports on other parameters such as chain length and charge density/patterning, for which, to the best of our knowledge, there has been little to no study on.

Rheological measurements have also highlighted the dramatic effect that increasing salt concentrations can have on the viscosity and/or relaxation behavior of complex

coacervates.^{111,137,139-143,145} This salt effect has been described in terms of the ability of salt to lower the activation energy barrier for the rearrangement of ion pairs using a “sticky” Rouse model.^{141,142} The specific chemical identity of the salt ions has also been shown to have a significant effect on both the phase behavior and the rheology of coacervates.^{8,145} These effects have largely been associated with Hofmeister-like effects that can be attributed to the ability of the various ions to affect the structure of water.¹⁴⁶⁻¹⁵⁰

We compared the effect of both the cation and the anion by testing a series of alkali halide salts at 10 mM concentration with the system of (EG)₂₅ and (KG)₂₅. By merely changing the identity of the salt ions we observed a dramatic acceleration in the time needed for our samples to equilibrate. KBr had the fastest average elapsed time of 5.0 min, followed by 35.0 min for NaBr, 57.5 min for KCl, and NaCl at 62.5 min (Figure 6b). Interestingly, the result for NaCl was comparable to what was seen with no added salt (Figures 5, S9d, and S10d).

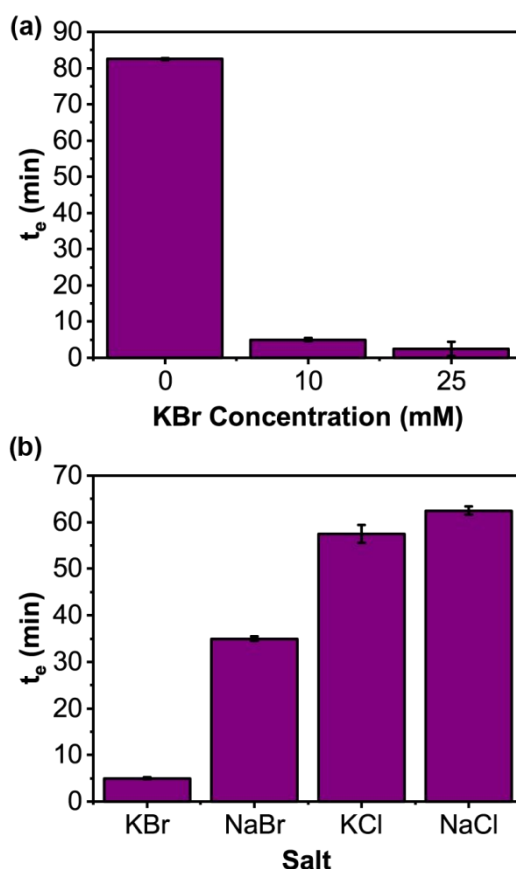


Figure 6. (a) The effect of increasing salt concentration with KBr on the average elapsed time of (EG)₂₅/(KG)₂₅, and (b) the effect of varying alkali halide salts at 10 mM and using the same system. Error bars represent the propagated error.

Our trends parallel rheological data reported by Sadman *et al.*, who used quartz crystal microbalance (QCM) studies to characterize thin films of poly(4-styrenesulfonic acid, sodium salt) (PSS) and poly(diallyldimethyl ammonium chloride) (PDADMAC).¹⁴⁵ The QCM data showed that the salt-induced changes in the modulus of the films correlated with the ability of the individual salts to bring water into the film. These results are particularly interesting as the trends of ($\text{Br}^- < \text{Cl}^-$ and $\text{K}^+ < \text{Na}^+$) and those from Sadman *et al.*, correlate with a decrease in the

hydration of the ions while resulting in an overall increase in the amount of water brought into the coacervate. More work is needed to better understand this phenomenon.

Conclusions:

We developed a turbidimetric method that uses small volumes and poor mixing to track the equilibration of a panel of complex coacervate samples prepared across a range of charge stoichiometries. Whereas a “well-mixed” experiment would be expected to result in a turbidity signal that is peaked at a 1:1 charge stoichiometry, corresponding to net neutrality, we saw a shift in the turbidity signal to net negative or net positive stoichiometries, depending on the order of polymer addition. The location of this peak could then be tracked over time as it shifted towards the expected 1:1 stoichiometry to identify a characteristic time scale for equilibration.

Analysis of the equilibration time for coacervates formed from polymers with increasing chain length demonstrated the ability of this method to probe both diffusion and frictional effects associated with the electrostatic interactions driving coacervation. The addition of salt or a zwitterionic buffer served to decrease the inter-chain friction, accelerating equilibration. Interestingly, we observed marked differences in the frictional interactions between polypeptides with asymmetric patterns of charge, depending on the order of polymer addition.

This method has the potential to provide insight into differences in the associative interactions present in different coacervate formulations. While not a replacement for more advanced techniques such as rheology that can more accurately and quantitatively probe the internal structure and dynamics of a material, the ability to perform simple characterizations with extremely low sample requirements in parallel with ongoing turbidimetric studies could help to serve as a screening tool to identify interesting and unique phenomena for further study.

Acknowledgements:

W.C.B.M. was supported by a Fellowship from the Soft Materials for Life Sciences National Research Traineeship Program #NRT-1545399. The authors would also like to thank Prof. Charles E. Sing, Prof. David Hoagland, Dr. Matthew Langer, and Xianci Zeng for helpful discussions.

References:

- (1) Sing, C. E.; Perry, S. L. Recent progress in the science of complex coacervation. *Soft Matter* **2020**, *50*, 9528–9530 DOI: 10.1039/D0SM00001A.
- (2) Blocher McTigue, W. C.; Perry, S. L. Protein Encapsulation Using Complex Coacervates: What Nature Has to Teach Us. *Small* **2020**, *111*, e1907671 DOI: 10.1002/sml.201907671.
- (3) Timilsena, Y. P.; Akanbi, T. O.; Khalid, N.; Adhikari, B.; Barrow, C. J. Complex coacervation: Principles, mechanisms and applications in microencapsulation. *Int. J. Biol. Macromol.* **2019**, *121* (C), 1276–1286 DOI: 10.1016/j.ijbiomac.2018.10.144.
- (4) Eratte, D.; Dowling, K.; Barrow, C. J.; Adhikari, B. Recent advances in the microencapsulation of omega-3 oil and probiotic bacteria through complex coacervation—A review. *Trends Food Sci Technol* **2018**, *71*, 121–131 DOI: 10.1016/j.tifs.2017.10.014.
- (5) Pathak, J.; Priyadarshini, E.; Rawat, K.; Bohidar, H. B. Complex coacervation in charge complementary biopolymers: Electrostatic versus surface patch binding. *Adv. Colloid Interface Sci.* **2017**, *250* (C), 40–53 DOI: 10.1016/j.cis.2017.10.006.
- (6) Blocher, W. C.; Perry, S. L. Complex coacervate-based materials for biomedicine. *WIREs Nanomed Nanobiotechnol* **2017**, *9*, e1442 DOI: 10.1002/wnan.1442.
- (7) Veis, A. A review of the early development of the thermodynamics of the complex coacervation phase separation. *Adv. Colloid Interface Sci.* **2011**, *167*, 2–11 DOI: 10.1016/j.cis.2011.01.007.
- (8) Perry, S.; Li, Y.; Priftis, D.; Leon, L.; Tirrell, M. The effect of salt on the complex coacervation of vinyl polyelectrolytes. *Polymers* **2014**, *6* (6), 1756–1772 DOI: 10.3390/polym6061756.
- (9) Priftis, D.; Leon, L.; Song, Z.; Perry, S. L.; Margossian, K. O.; Tropnikova, A.; Cheng, J.; Tirrell, M. Self-assembly of α -helical polypeptides driven by complex coacervation. *Angew. Chem.* **2015**, *127* (38), 11280–11284 DOI: 10.1002/ange.201504861.
- (10) Hoffmann, K. Q.; Perry, S. L.; Leon, L.; Priftis, D.; Tirrell, M.; de Pablo, J. J. A molecular view of the role of chirality in charge-driven polypeptide complexation. *Soft Matter* **2015**, *11* (8), 1525–1538 DOI: 10.1039/C4SM02336F.
- (11) Water, J. J.; Schack, M. M.; Velazquez-Campoy, A.; Maltesen, M. J.; van de Weert, M.; Jorgensen, L. Complex coacervates of hyaluronic acid and lysozyme: Effect on protein structure and physical stability. **2014**, *88* (2), 325–331 DOI: 10.1016/j.ejpb.2014.09.001.
- (12) Black, K. A.; Priftis, D.; Perry, S. L.; Yip, J.; Byun, W. Y.; Tirrell, M. Protein encapsulation via polypeptide complex coacervation. *ACS Macro Lett.* **2014**, *3* (10), 1088–1091 DOI: 10.1021/mz500529v.
- (13) Perry, S. L.; Leon, L.; Hoffmann, K. Q.; Kade, M. J.; Priftis, D.; Black, K. A.; Wong, D.; Klein, R. A.; Pierce, C. F.; Margossian, K. O.; et al. Chirality-selected phase behaviour in ionic polypeptide complexes. *Nat Commun* **2015**, *6* (1), 6052 DOI: 10.1038/ncomms7052.
- (14) Priftis, D.; Xia, X.; Margossian, K. O.; Perry, S. L.; Leon, L.; Qin, J.; de Pablo, J. J.; Tirrell, M. Ternary, tunable polyelectrolyte complex fluids driven by complex coacervation. *Macromolecules* **2014**, *47* (9), 3076–3085 DOI: 10.1021/ma500245j.
- (15) Perry, S. L.; Neumann, S. G.; Neumann, T.; Cheng, K.; Ni, J.; Weinstein, J. R.; Schaffer, D. V.; Tirrell, M. Challenges in nucleic acid-lipid films for transfection. *AIChE J.* **2013**, *59* (9), 3203–3213 DOI: 10.1002/aic.14198.

- (16) Priftis, D.; Megley, K.; Laugel, N.; Tirrell, M. Complex coacervation of poly(ethyleneimine)/polypeptide aqueous solutions: thermodynamic and rheological characterization. *J. Colloid Interface Sci.* **2013**, *398*, 39–50 DOI: 10.1016/j.jcis.2013.01.055.
- (17) Chollakup, R.; Smitthipong, W.; Eisenbach, C. D.; Tirrell, M. Phase Behavior and Coacervation of Aqueous Poly(acrylic acid)–Poly(allylamine) Solutions. *Macromolecules* **2010**, *43* (5), 2518–2528 DOI: 10.1021/ma902144k.
- (18) Chollakup, R.; Beck, J. B.; Dirnberger, K.; Tirrell, M.; Eisenbach, C. D. Polyelectrolyte molecular weight and salt effects on the phase behavior and coacervation of aqueous solutions of poly(acrylic acid) sodium salt and poly(allylamine) hydrochloride. *Macromolecules* **2013**, *46* (6), 2376–2390 DOI: 10.1021/ma202172q.
- (19) Priftis, D.; Farina, R.; Tirrell, M. Interfacial Energy of Polypeptide Complex Coacervates Measured via Capillary Adhesion†. *Langmuir* **2012**, *28* (23), 8721–8729 DOI: 10.1021/la300769d.
- (20) Priftis, D.; Tirrell, M. Phase behaviour and complex coacervation of aqueous polypeptide solutions. *Soft Matter* **2012**, *8* (36), 9396–9405 DOI: 10.1039/C2SM25604E.
- (21) Priftis, D.; Laugel, N.; Tirrell, M. Thermodynamic characterization of polypeptide complex coacervation. *Langmuir* **2012**, *28* (45), 15947–15957 DOI: 10.1021/la302729r.
- (22) Xu, A. Y.; Melton, L. D.; Ryan, T. M.; Mata, J. P.; Rekas, A.; Williams, M. A. K.; McGillivray, D. J. Effects of polysaccharide charge pattern on the microstructures of beta-lactoglobulin-pectin complex coacervates, studied by SAXS and SANS. *Food Hydrocolloids* **2018**, *77*, 952–963 DOI: 10.1016/j.foodhyd.2017.11.045.
- (23) Xiong, W.; Ren, C.; Tian, M.; Yang, X.; Li, J.; Bin Li. Complex coacervation of ovalbumin-carboxymethylcellulose assessed by isothermal titration calorimeter and rheology: Effect of ionic strength and charge density of polysaccharide. *Food Hydrocolloids* **2017**, *73*, 41–50 DOI: 10.1016/j.foodhyd.2017.06.031.
- (24) de Souza, V. B.; Thomazini, M.; Barrientos, M. A. E.; Nalin, C. M.; Ferro-Furtado, R.; Genovese, M. I.; Favaro-Trindade, C. S. Functional properties and encapsulation of a proanthocyanidin-rich cinnamon extract (*Cinnamomum zeylanicum*) by complex coacervation using gelatin and different polysaccharides. *Food Hydrocolloids* **2017**, 1–10 DOI: 10.1016/j.foodhyd.2017.09.040.
- (25) Frankel, E. A.; Bevilacqua, P. C.; Keating, C. D. Polyamine/Nucleotide coacervates provide strong compartmentalization of Mg²⁺, nucleotides, and RNA. *Langmuir* **2016**, *32* (8), 2041–2049 DOI: 10.1021/acs.langmuir.5b04462.
- (26) Knaapila, M.; Costa, T.; Garamus, V. M.; Kraft, M.; Drechsler, M.; Scherf, U.; Burrows, H. D. Polyelectrolyte complexes of a cationic all conjugated fluorene–thiophene diblock copolymer with aqueous DNA. *J. Phys. Chem. B* **2015**, *119* (7), 3231–3241 DOI: 10.1021/jp5110032.
- (27) Arfin, N.; Aswal, V. K.; Bohidar, H. B. Overcharging, thermal, viscoelastic and hydration properties of DNA–gelatin complex coacervates: pharmaceutical and food industries. *RSC Adv.* **2014**, *4* (23), 11705–11709 DOI: 10.1039/c3ra46618c.
- (28) Tang, T. Y. D.; Antognozzi, M.; Vicary, J. A.; Perriman, A. W.; Mann, S. Small-molecule uptake in membrane-free peptide/nucleotide protocells. *Soft Matter* **2013**, *9* (31), 7647–7656 DOI: 10.1039/c3sm50726b.
- (29) Williams, D. S.; Koga, S.; Hak, C. R. C.; Majrekar, A.; Patil, A. J.; Perriman, A. W.;

- Mann, S. Polymer/nucleotide droplets as bio-inspired functional micro-compartments. *Soft Matter* **2012**, *8* (22), 6004–6011 DOI: 10.1039/c2sm25184a.
- (30) Koga, S.; Williams, D. S.; Perriman, A. W.; Mann, S. Peptide-nucleotide microdroplets as a step towards a membrane-free protocell model. *Nat Chem* **2011**, *3* (9), 720–724 DOI: 10.1038/nchem.1110.
- (31) Kawamura, A.; Harada, A.; Kono, K.; Kataoka, K. Self-Assembled Nano-Bioreactor from Block Ionomers with Elevated and Stabilized Enzymatic Function. *Bioconjugate Chem.* **2007**, *18* (5), 1555–1559 DOI: 10.1021/bc070029t.
- (32) Jaturanpinyo, M.; Harada, A.; Yuan, X.; Kataoka, K. Preparation of Bionanoreactor Based on Core–Shell Structured Polyion Complex Micelles Entrapping Trypsin in the Core Cross-Linked with Glutaraldehyde. *Bioconjugate Chem.* **2004**, *15* (2), 344–348 DOI: 10.1021/bc034149m.
- (33) Harada, A.; Kataoka, K. Pronounced activity of enzymes through the incorporation into the core of polyion complex micelles made from charged block copolymers. *J. Controlled Release* **2001**, *72* (1-3), 85–91 DOI: 10.1016/S0168-3659(01)00264-4.
- (34) Kataoka, K.; Harada, A.; Nagasaki, Y. Block copolymer micelles for drug delivery: design, characterization and biological significance. *Adv. Drug Delivery Rev.* **2001**, *47*, 113–131.
- (35) Harada, A.; Kataoka, K. Novel Polyion Complex Micelles Entrapping Enzyme Molecules in the Core. 2. Characterization of the Micelles Prepared at Nonstoichiometric Mixing Ratios. *Langmuir* **1999**, *15* (12), 4208–4212 DOI: 10.1021/la981087t.
- (36) Harada, A.; Kataoka, K. Novel Polyion Complex Micelles Entrapping Enzyme Molecules in the Core: Preparation of Narrowly-Distributed Micelles from Lysozyme and Poly(ethylene glycol)-Poly(aspartic acid) Block Copolymer in Aqueous Medium. *Macromolecules* **1998**, *31*, 288–294.
- (37) Harada, A.; Kataoka, K. Formation of Polyion Complex Micelles in an Aqueous Milieu from a Pair of Oppositely-Charged Block Copolymers with Poly(ethylene glycol) Segments. *Macromolecules* **1995**, *28*, 5294–5299.
- (38) Voets, I. K.; de Keizer, A.; Cohen Stuart, M. A. Complex coacervate core micelles. *Adv. Colloid Interface Sci.* **2009**, *147-148* (C), 300–318 DOI: 10.1016/j.cis.2008.09.012.
- (39) Kayitmazer, A. B.; Seyrek, E.; Dubin, P. L.; Staggemeier, B. A. Influence of Chain Stiffness on the Interaction of Polyelectrolytes with Oppositely Charged Micelles and Proteins. *J. Phys. Chem. B* **2003**, *107* (32), 8158–8165 DOI: 10.1021/jp034065a.
- (40) Kalantar, T. H.; Tucker, C. J.; Zalusky, A. S.; Boomgaard, T. A.; Wilson, B. E.; Ladika, M.; Jordan, S. L.; Li, W. K.; Zhang, X.; Goh, C. G. High throughput workflow for coacervate formation and characterization in shampoo systems. *J. Cosmet. Sci.* **2007**, *58*, 375–383.
- (41) Hu, D.; Chou, K. C. Re-evaluating the surface tension analysis of polyelectrolyte-surfactant mixtures using phase-sensitive sum frequency generation spectroscopy. *J Am Chem Soc* **2014**, *136* (43), 15114–15117 DOI: 10.1021/ja5049175.
- (42) Nejati, M. M.; Khaledi, M. G. Perfluoro-alcohol-induced complex coacervates of polyelectrolyte–surfactant mixtures: Phase behavior and analysis. *Langmuir* **2015**, *31* (20), 5580–5589 DOI: 10.1021/acs.langmuir.5b00444.
- (43) Szczepanowicz, K.; Bazylińska, U.; Pietkiewicz, J.; Szyk-Warszyńska, L.; Wilk, K. A.;

- Warszyński, P. Biocompatible long-sustained release oil-core polyelectrolyte nanocarriers: From controlling physical state and stability to biological impact. *Adv. Colloid Interface Sci.* **2015**, *222* (C), 678–691 DOI: 10.1016/j.cis.2014.10.005.
- (44) Wang, Y.; Kimura, K.; Huang, Q.; Dubin, P. L.; Jaeger, W. Effects of Salt on Polyelectrolyte–Micelle Coacervation. *Macromolecules* **1999**, *32* (21), 7128–7134 DOI: 10.1021/ma990972v.
- (45) Wang, W.; Mauroy, H.; Zhu, K.; Knudsen, K. D.; Kjøniksen, A.-L.; Nyström, B.; Sande, S. A. Complex coacervate micelles formed by a C18-capped cationic triblock thermoresponsive copolymer interacting with SDS. *Soft Matter* **2012**, *8* (45), 11514–11525 DOI: 10.1039/c2sm26567b.
- (46) Karimi, F.; Qazvini, N. T.; Namivandi-Zangeneh, R. Fish gelatin/laponite biohybrid elastic coacervates: a complexation kinetics–structure relationship study. *Int. J. Biol. Macromol.* **2013**, *61*, 102–113 DOI: 10.1016/j.ijbiomac.2013.06.054.
- (47) Pawar, N.; Bohidar, H. B. Anisotropic domain growth and complex coacervation in nanoclay-polyelectrolyte solutions. *Adv. Colloid Interface Sci.* **2011**, *167* (1-2), 12–23 DOI: 10.1016/j.cis.2011.06.007.
- (48) Krogstad, D. V.; Lynd, N. A.; Choi, S.-H.; Spruell, J. M.; Hawker, C. J.; Kramer, E. J.; Tirrell, M. V. Effects of polymer and salt concentration on the structure and properties of triblock copolymer coacervate hydrogels. *Macromolecules* **2013**, *46* (4), 1512–1518 DOI: 10.1021/ma302299r.
- (49) Krogstad, D. V.; Choi, S.-H.; Lynd, N. A.; Audus, D. J.; Perry, S. L.; Gopez, J. D.; Hawker, C. J.; Kramer, E. J.; Tirrell, M. V. Small angle neutron scattering study of complex coacervate micelles and hydrogels formed from ionic diblock and triblock copolymers. *J. Phys. Chem. B* **2014**, *118* (45), 13011–13018 DOI: 10.1021/jp509175a.
- (50) Krogstad, D. V.; Lynd, N. A.; Miyajima, D.; Gopez, J.; Hawker, C. J.; Kramer, E. J.; Tirrell, M. V. Structural evolution of polyelectrolyte complex core micelles and ordered-phase bulk materials. *Macromolecules* **2014**, *47* (22), 8026–8032 DOI: 10.1021/ma5017852.
- (51) Hunt, J. N.; Feldman, K. E.; Lynd, N. A.; Deek, J.; Campos, L. M.; Spruell, J. M.; Hernandez, B. M.; Kramer, E. J.; Hawker, C. J. Tunable, High Modulus Hydrogels Driven by Ionic Coacervation. *Adv. Mater.* **2011**, *23* (20), 2327–2331 DOI: 10.1002/adma.201004230.
- (52) Stewart-Sloan, C. R.; Olsen, B. D. Protonation-induced microphase separation in thin films of a polyelectrolyte-hydrophilic diblock copolymer. *ACS Macro Lett.* **2014**, *3* (5), 410–414 DOI: 10.1021/mz400650q.
- (53) Kim, B.; Lam, C. N.; Olsen, B. D. Nanopatterned Protein Films Directed by Ionic Complexation with Water-Soluble Diblock Copolymers. *Macromolecules* **2012**, *45* (11), 4572–4580 DOI: 10.1021/ma2024914.
- (54) Wu, F.-G.; Jiang, Y.-W.; Chen, Z.; Yu, Z.-W. Folding behaviors of protein (lysozyme) confined in polyelectrolyte complex micelle. *Langmuir* **2016**, *32* (15), 3655–3664 DOI: 10.1021/acs.langmuir.6b00235.
- (55) Ishii, S.; Kaneko, J.; Nagasaki, Y. Development of a long-acting, protein-loaded, redox-active, injectable gel formed by a polyion complex for local protein therapeutics. *Biomaterials* **2016**, *84* (C), 210–218 DOI: 10.1016/j.biomaterials.2016.01.029.

- (56) Hwang, D. S.; Waite, J. H.; Tirrell, M. Promotion of osteoblast proliferation on complex coacervation-based hyaluronic acid–recombinant mussel adhesive protein coatings on titanium. *Biomaterials* **2010**, *31* (6), 1080–1084 DOI: 10.1016/j.biomaterials.2009.10.041.
- (57) Wang, W.; Xu, Y.; Li, A.; Li, T.; Liu, M.; Klitzing, von, R.; Ober, C. K.; Kayitmazer, A. B.; Li, L.; Guo, X. Zinc induced polyelectrolyte coacervate bioadhesive and its transition to a self-healing hydrogel. *RSC Adv.* **2015**, *5* (82), 66871–66878 DOI: 10.1039/C5RA11915D.
- (58) Winslow, B. D.; Shao, H.; Stewart, R. J.; Tresco, P. A. Biocompatibility of adhesive complex coacervates modeled after the sandcastle glue of *Phragmatopoma californica* for craniofacial reconstruction. *Biomaterials* **2010**, *31* (36), 9373–9381 DOI: 10.1016/j.biomaterials.2010.07.078.
- (59) Favi, P. M.; Yi, S.; Lenaghan, S. C.; Xia, L.; Zhang, M. Inspiration from the natural world: from bio-adhesives to bio-inspired adhesives. *J. Adhes. Sci. Technol.* **2013**, *28* (3-4), 290–319 DOI: 10.1080/01694243.2012.691809.
- (60) Mann, L. K.; Papanna, R.; Moise, K. J., Jr; Byrd, R. H.; Popek, E. J.; Kaur, S.; Tseng, S. C. G.; Stewart, R. J. Fetal membrane patch and biomimetic adhesive coacervates as a sealant for fetoscopic defects. *Acta Biomater.* **2012**, *8* (6), 2160–2165 DOI: 10.1016/j.actbio.2012.02.014.
- (61) Lim, S.; Choi, Y. S.; Kang, D. G.; Song, Y. H.; Cha, H. J. The adhesive properties of coacervated recombinant hybrid mussel adhesive proteins. *Biomaterials* **2010**, *31* (13), 3715–3722 DOI: 10.1016/j.biomaterials.2010.01.063.
- (62) Hwang, D. S.; Zeng, H.; Srivastava, A.; Krogstad, D. V.; Tirrell, M.; Israelachvili, J. N.; Waite, J. H. Viscosity and interfacial properties in a mussel-inspired adhesive coacervate. *Soft Matter* **2010**, *6* (14), 3232–3235 DOI: 10.1039/c002632h.
- (63) Hwang, D. S.; Zeng, H.; Lu, Q.; Israelachvili, J.; Waite, J. H. Adhesion mechanism in a DOPA-deficient foot protein from green mussels. *Soft Matter* **2012**, *8* (20), 5640–5649 DOI: 10.1039/c2sm25173f.
- (64) Kaur, S.; Weerasekare, G. M.; Stewart, R. J. Multiphase Adhesive Coacervates Inspired by the Sandcastle Worm. *ACS Appl. Mater. Interfaces* **2011**, *3* (4), 941–944 DOI: 10.1021/am200082v.
- (65) Ahn, B. K.; Das, S.; Linstadt, R.; Kaufman, Y.; Martinez-Rodriguez, N. R.; Mirshafian, R.; Kesselman, E.; Talmon, Y.; Lipshutz, B. H.; Israelachvili, J. N.; et al. High-performance mussel-inspired adhesives of reduced complexity. *Nat Commun* **2015**, *6* (1), 8663 DOI: 10.1038/ncomms9663.
- (66) Stewart, R. J.; Wang, C. S.; Shao, H. Complex coacervates as a foundation for synthetic underwater adhesives. *Adv. Colloid Interface Sci.* **2011**, *167* (1-2), 85–93 DOI: 10.1016/j.cis.2010.10.009.
- (67) Choi, Y. S.; Kang, D. G.; Lim, S.; Yang, Y. J.; Kim, C. S.; Cha, H. J. Recombinant mussel adhesive protein fp-5 (MAP fp-5) as a bulk bioadhesive and surface coating material. *Biofouling* **2011**, *27* (7), 729–737 DOI: 10.1080/08927014.2011.600830.
- (68) Shao, H.; Bachus, K. N.; Stewart, R. J. A Water-Borne Adhesive Modeled after the Sandcastle Glue of *P. californica*. *Macromol. Biosci.* **2009**, *9* (5), 464–471 DOI: 10.1002/mabi.200800252.
- (69) Lim, S.; Moon, D.; Kim, H. J.; Seo, J. H.; Kang, I. S.; Cha, H. J. Interfacial tension of

- complex coacervated mussel adhesive protein according to the Hofmeister series. *Langmuir* **2014**, *30* (4), 1108–1115 DOI: 10.1021/la403680z.
- (70) Shao, H.; Weerasekare, G. M.; Stewart, R. J. Controlled curing of adhesive complex coacervates with reversible periodate carbohydrate complexes. *J. Biomed. Mater. Res., Part A* **2011**, *97A* (1), 46–51 DOI: 10.1002/jbm.a.33026.
- (71) Farrar, D. F. Bone adhesives for trauma surgery A review of challenges and developments. *Int. J. Adhes. Adhes.* **2012**, *33* (C), 89–97 DOI: 10.1016/j.ijadhadh.2011.11.009.
- (72) Pippa, N.; Karayianni, M.; Pispas, S.; Demetzos, C. Complexation of cationic-neutral block polyelectrolyte with insulin and in vitro release studies. *Int. J. Pharm.* **2015**, *491* (1–2), 136–143 DOI: 10.1016/j.ijpharm.2015.06.013.
- (73) Pippa, N.; Kalinova, R.; Dimitrov, I.; Pispas, S.; Demetzos, C. Insulin/poly(ethylene glycol)-block-poly(L-lysine) Complexes: Physicochemical Properties and Protein Encapsulation. *J. Phys. Chem. B* **2015**, *119* (22), 6813–6819 DOI: 10.1021/acs.jpcc.5b01664.
- (74) Nolles, A.; Westphal, A. H.; de Hoop, J. A.; Fokkink, R. G.; Kleijn, J. M.; van Berkel, W. J. H.; Borst, J. W.; Westphal, A. H. Encapsulation of GFP in complex coacervate core micelles. *Biomacromolecules* **2015**, *16* (5), 1542–1549 DOI: 10.1021/acs.biomac.5b00092.
- (75) Lindhoud, S.; de Vries, R.; Norde, W.; Cohen Stuart, M. A. Structure and Stability of Complex Coacervate Core Micelles with Lysozyme. *Biomacromolecules* **2007**, *8* (7), 2219–2227 DOI: 10.1021/bm0700688.
- (76) Lindhoud, S.; Claessens, M. M. A. E. Accumulation of small protein molecules in a macroscopic complex coacervate. *Soft Matter* **2016**, *12* (2), 408–413 DOI: 10.1039/C5SM02386F.
- (77) Chen, W. C. W.; Lee, B. G.; Park, D. W.; Kim, K.; Chu, H.; Kim, K.; Huard, J.; Wang, Y. Controlled dual delivery of fibroblast growth factor-2 and Interleukin-10 by heparin-based coacervate synergistically enhances ischemic heart repair. *Biomaterials* **2015**, *72* (c), 138–151 DOI: 10.1016/j.biomaterials.2015.08.050.
- (78) Kishimura, A.; Koide, A.; Osada, K.; Yamasaki, Y.; Kataoka, K. Encapsulation of Myoglobin in PEGylated Polyion Complex Vesicles Made from a Pair of Oppositely Charged Block Ionomers: A Physiologically Available Oxygen Carrier. *Angew. Chem. Int. Ed.* **2007**, *46* (32), 6085–6088 DOI: 10.1002/anie.200701776.
- (79) Lindhoud, S.; de Vries, R.; Schweins, R.; Cohen Stuart, M. A.; Norde, W. Salt-induced release of lipase from polyelectrolyte complex micelles. *Soft Matter* **2009**, *5* (1), 242–250 DOI: 10.1039/B811640G.
- (80) Lindhoud, S.; Norde, W.; Cohen Stuart, M. A. Reversibility and Relaxation Behavior of Polyelectrolyte Complex Micelle Formation. *J. Phys. Chem. B* **2009**, *113* (16), 5431–5439 DOI: 10.1021/jp809489f.
- (81) Chu, H.; Gao, J.; Chen, C.-W.; Huard, J.; Wang, Y. Injectable fibroblast growth factor-2 coacervate for persistent angiogenesis. *PNAS* **2011**, *108* (33), 13444–13449 DOI: 10.1073/pnas.1110121108.
- (82) Johnson, N. R.; Ambe, T.; Wang, Y. Lysine-based polycation:heparin coacervate for controlled protein delivery. *Acta Biomater.* **2014**, *10* (1), 40–46 DOI: 10.1016/j.actbio.2013.09.012.

- (83) Chu, H.; Chen, C.-W.; Huard, J.; Wang, Y. The effect of a heparin-based coacervate of fibroblast growth factor-2 on scarring in the infarcted myocardium. *Biomaterials* **2013**, *34* (6), 1747–1756 DOI: 10.1016/j.biomaterials.2012.11.019.
- (84) Yen, J.; Ying, H.; Wang, H.; Yin, L.; Uckun, F.; Cheng, J. CD44 mediated nonviral gene delivery into human embryonic stem cells via hyaluronic-acid-coated nanoparticles. *ACS Biomater. Sci. Eng.* **2016**, *2* (3), 326–335 DOI: 10.1021/acsbiomaterials.5b00393.
- (85) Kuo, C.-H.; Leon, L.; Chung, E. J.; Huang, R.-T.; Sontag, T. J.; Reardon, C. A.; Getz, G. S.; Tirrell, M.; Fang, Y. Inhibition of atherosclerosis-promoting microRNAs via targeted polyelectrolyte complex micelles. *J. Mater. Chem. B* **2014**, *2*, 8142–8153 DOI: 10.1039/C4TB00977K.
- (86) Aumiller, W. M., Jr; Keating, C. D. Phosphorylation-mediated RNA/peptide complex coacervation as a model for intracellular liquid organelles. *Nat Chem* **2015**, *8* (2), 129–137 DOI: 10.1038/nchem.2414.
- (87) Jin, K.-M.; Kim, Y.-H. Injectable, thermo-reversible and complex coacervate combination gels for protein drug delivery. *J. Controlled Release* **2008**, *127* (3), 249–256 DOI: 10.1016/j.jconrel.2008.01.015.
- (88) Kinoh, H.; Miura, Y.; Chida, T.; Liu, X.; Mizuno, K.; Fukushima, S.; Morodomi, Y.; Nishiyama, N.; Cabral, H.; Kataoka, K. Nanomedicines eradicating cancer stem-like cells in vivo by pH-triggered intracellular cooperative action of loaded drugs. *ACS Nano* **2016**, *10* (6), 5643–5655 DOI: 10.1021/acs.nano.6b00900.
- (89) Anraku, Y.; Kishimura, A.; Kamiya, M.; Tanaka, S.; Nomoto, T.; Toh, K.; Matsumoto, Y.; Fukushima, S.; Sueyoshi, D.; Kano, M. R.; et al. Systemically injectable enzyme-loaded polyion complex vesicles as in vivo nanoreactors functioning in tumors. *Angew. Chem.* **2015**, *128* (2), 570–575 DOI: 10.1002/ange.201508339.
- (90) Schoonen, L.; van Hest, J. C. M. Compartmentalization approaches in soft matter science: From nanoreactor development to organelle mimics. *Adv. Mater.* **2015**, *28* (6), 1109–1128 DOI: 10.1002/adma.201502389.
- (91) Lv, K.; Perriman, A. W.; Mann, S. Photocatalytic multiphase micro-droplet reactors based on complex coacervation. *Chem. Commun.* **2015**, *51* (41), 8600–8602 DOI: 10.1039/C5CC01914A.
- (92) Hyman, A. A.; Simons, K. Beyond Oil and Water--Phase Transitions in Cells. *Science* **2012**, *337* (6098), 1047–1049 DOI: 10.1126/science.1223728.
- (93) Hyman, A. A.; Brangwynne, C. P. Beyond Stereospecificity: Liquids and Mesoscale Organization of Cytoplasm. *Dev. Cell* **2011**, *21* (1), 14–16 DOI: 10.1016/j.devcel.2011.06.013.
- (94) Weber, S. C.; Brangwynne, C. P. Getting RNA and Protein in Phase. *Cell* **2012**, *149* (6), 1188–1191 DOI: 10.1016/j.cell.2012.05.022.
- (95) Elbaum-Garfinkle, S.; Kim, Y.; Szczepaniak, K.; Chen, C. C.-H.; Eckmann, C. R.; Myong, S.; Brangwynne, C. P. The disordered P granule protein LAF-1 drives phase separation into droplets with tunable viscosity and dynamics. *PNAS* **2015**, *112* (23), 7189–7194 DOI: 10.1073/pnas.1504822112.
- (96) Kato, M.; Han, T. W.; Xie, S.; Shi, K.; Du, X.; Wu, L. C.; Mirzaei, H.; Goldsmith, E. J.; Longgood, J.; Pei, J.; et al. Cell-free Formation of RNA Granules: Low Complexity Sequence Domains Form Dynamic Fibers within Hydrogels. *Cell* **2012**, *149* (4), 753–767

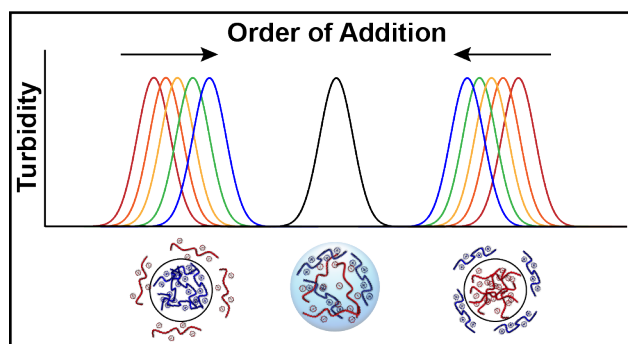
- DOI: 10.1016/j.cell.2012.04.017.
- (97) Eulalio, A.; Behm-Ansmant, I.; Izaurralde, E. P bodies: at the crossroads of post-transcriptional pathways. *Nat. Rev. Mol. Cell Biol.* **2007**, *8* (1), 9–22 DOI: 10.1038/nrm2080.
- (98) Han, T. W.; Kato, M.; Xie, S.; Wu, L. C.; Mirzaei, H.; Pei, J.; Chen, M.; Xie, Y.; Allen, J.; Xiao, G.; et al. Cell-free Formation of RNA Granules: Bound RNAs Identify Features and Components of Cellular Assemblies. *Cell* **2012**, *149* (4), 768–779 DOI: 10.1016/j.cell.2012.04.016.
- (99) Jia, T. Z.; Hentrich, C.; Szostak, J. W. Rapid RNA exchange in aqueous two-phase system and coacervate droplets. *Origins Life Evol. Biospheres* **2014**, *44* (1), 1–12 DOI: 10.1007/s11084-014-9355-8.
- (100) Li, P.; Banjade, S.; Cheng, H.-C.; Kim, S.; Chen, B.; Guo, L.; Llaguno, M.; Hollingsworth, J. V.; King, D. S.; Banani, S. F.; et al. Phase transitions in the assembly of multivalent signalling proteins. *Nature* **2012**, *483* (7389), 336–340 DOI: 10.1038/nature10879.
- (101) Walter, H. Consequences of Phase Separation in Cytoplasm. *Int. Rev. Cytol.* **1999**, *192*, 331–343.
- (102) Brangwynne, C. P.; Mitchison, T. J.; Hyman, A. A. Active liquid-like behavior of nucleoli determines their size and shape in *Xenopus laevis* oocytes. *PNAS* **2011**, *108* (11), 4334–4339 DOI: 10.1073/pnas.1017150108.
- (103) Brangwynne, C. P.; Eckmann, C. R.; Courson, D. S.; Rybarska, A.; Hoege, C.; Gharakhani, J.; Julicher, F.; Hyman, A. A. Germline P Granules Are Liquid Droplets That Localize by Controlled Dissolution/Condensation. *Science* **2009**, *324* (5935), 1729–1732 DOI: 10.1126/science.1172046.
- (104) Brangwynne, C. P. Phase transitions and size scaling of membrane-less organelles. *J. Cell. Biol.* **2013**, *203* (6), 875–881 DOI: 10.1083/jcb.201308087.
- (105) Zhang, H.; Elbaum-Garfinkle, S.; Langdon, E. M.; Taylor, N.; Occhipinti, P.; Bridges, A. A.; Brangwynne, C. P.; Gladfelter, A. S. RNA controls PolyQ protein phase transitions. *Mol. Cell* **2015**, *60* (2), 220–230 DOI: 10.1016/j.molcel.2015.09.017.
- (106) Lin, Y.; Protter, D. S. W.; Rosen, M. K.; Parker, R. Formation and maturation of phase-separated liquid droplets by RNA-binding proteins. *Mol. Cell* **2015**, *60* (2), 208–219 DOI: 10.1016/j.molcel.2015.08.018.
- (107) Fromm, S. A.; Kamenz, J.; Nöldeke, E. R.; Neu, A.; Zocher, G.; Sprangers, R. In vitro reconstitution of a cellular phase-transition process that involves the mRNA decapping machinery. *Angew. Chem. Int. Ed.* **2014**, *53* (28), 7354–7359 DOI: 10.1002/anie.201402885.
- (108) Patel, A.; Lee, H. O.; Jawerth, L.; Maharana, S.; Jahnel, M.; Hein, M. Y.; Stoyanov, S.; Mahamid, J.; Saha, S.; Franzmann, T. M.; et al. A liquid-to-solid phase transition of the ALS protein FUS accelerated by disease mutation. *Cell* **2015**, *162* (5), 1066–1077 DOI: 10.1016/j.cell.2015.07.047.
- (109) Burke, K. A.; Janke, A. M.; Rhine, C. L.; Fawzi, N. L. Residue-by-residue view of in vitro FUS granules that bind the C-terminal domain of RNA polymerase II. *Mol. Cell* **2015**, *60* (2), 231–241 DOI: 10.1016/j.molcel.2015.09.006.
- (110) Radhakrishna, M.; Basu, K.; Liu, Y.; Shamsi, R.; Perry, S. L.; Sing, C. E. Molecular

- Connectivity and Correlation Effects on Polymer Coacervation. *Macromolecules* **2017**, *50* (7), 3030–3037 DOI: 10.1021/acs.macromol.6b02582.
- (111) Liu, Y.; Momani, B.; Winter, H. H.; Perry, S. L. Rheological characterization of liquid-to-solid transitions in bulk polyelectrolyte complexes. *Soft Matter* **2017**, *13*, 7332–7340 DOI: 10.1039/C7SM01285C.
- (112) Spruijt, E.; Westphal, A. H.; Borst, J. W.; Cohen Stuart, M. A.; van der Gucht, J. Binodal Compositions of Polyelectrolyte Complexes. *Macromolecules* **2010**, *43* (15), 6476–6484 DOI: 10.1021/ma101031t.
- (113) Huang, J.; Morin, F. J.; Laaser, J. E. Charge-Density-Dominated Phase Behavior and Viscoelasticity of Polyelectrolyte Complex Coacervates. *Macromolecules* **2019**, *52* (13), 4957–4967 DOI: 10.1021/acs.macromol.9b00036.
- (114) Lou, J.; Friedowitz, S.; Qin, J.; Xia, Y. Tunable Coacervation of Well-Defined Homologous Polyanions and Polycations by Local Polarity. *ACS Cent Sci* **2019**, *5* (3), 549–557 DOI: 10.1021/acscentsci.8b00964.
- (115) Kapelner, R. A.; Obermeyer, A. C. Ionic polypeptide tags for protein phase separation. *Chem. Sci.* **2019**, *10* (9), 2700–2707 DOI: 10.1039/C8SC04253E.
- (116) Cummings, C. S.; Obermeyer, A. C. Phase Separation Behavior of Supercharged Proteins and Polyelectrolytes. *Biochemistry* **2018**, *57* (3), 314–323 DOI: 10.1021/acs.biochem.7b00990.
- (117) Comert, F.; Dubin, P. L. Liquid-liquid and liquid-solid phase separation in protein-polyelectrolyte systems. *Adv. Colloid Interface Sci.* **2017**, *239*, 213–217 DOI: 10.1016/j.cis.2016.08.005.
- (118) Niu, F.; Dong, Y.; Shen, F.; Wang, J.; Liu, Y.; Su, Y.; Xu, R.; Wang, J.; Yang, Y. Phase separation behavior and structural analysis of ovalbumin-gum arabic complex coacervation. *Food Hydrocolloids* **2015**, *43* (C), 1–7 DOI: 10.1016/j.foodhyd.2014.02.009.
- (119) Takahashi, R.; Narayanan, T.; Sato, T. Growth Kinetics of Polyelectrolyte Complexes Formed from Oppositely-Charged Homopolymers Studied by Time-Resolved Ultra-Small-Angle X-ray Scattering. *J Phys Chem Lett* **2017**, 737–741 DOI: 10.1021/acs.jpcclett.6b02957.
- (120) Su, C.; Zhao, M.; Zhu, Z.; Zhou, J.; Wen, H.; Yin, Y.; Deng, Y.; Qiu, D.; Li, B.; Liang, D. Effect of Peptide Charge Distribution on the Structure and Kinetics of DNA Complex. *Macromolecules* **2015**, *48* (3), 756–763 DOI: 10.1021/ma501901b.
- (121) Salehi, A.; Desai, P. S.; Li, J.; Steele, C. A.; Larson, R. G. Relationship between Polyelectrolyte Bulk Complexation and Kinetics of Their Layer-by-Layer Assembly. *Macromolecules* **2015**, *48*, 400–409 DOI: 10.1021/ma502273a.
- (122) Salvatore, D.; Croguennec, T.; Bouhallab, S.; Forge, V.; Nicolai, T. Kinetics and Structure during Self-Assembly of Oppositely Charged Proteins in Aqueous Solution. *Biomacromolecules* **2011**, *12* (5), 1920–1926 DOI: 10.1021/bm200264m.
- (123) Kuehn, F.; Fischer, K.; Schmidt, M. Kinetics of Complex Formation between DNA and Cationically Charged Cylindrical Brush Polymers Observed by Stopped Flow Light Scattering. *Macromol. Rapid Commun.* **2009**, *30* (17), 1470–1476 DOI: 10.1002/marc.200900166.
- (124) Kanai, S.; Muthukumar, M. Phase separation kinetics of polyelectrolyte solutions. *J Chem*

- Phys* **2007**, *127* (24), 244908–244914 DOI: 10.1063/1.2806299.
- (125) Sato, H.; Seki, H. Kinetic Study on the Founcation of Polyelectrolyte Complexes. Poly(L-lysine hydrobromide) ad Poly(L-glutamate sodium salt). *Polymer J* **1993**, *25* (5), 529–533.
- (126) Liu, X.; Chapel, J.-P.; Schatz, C. Structure, thermodynamic and kinetic signatures of a synthetic polyelectrolyte coacervating system. *Adv. Colloid Interface Sci.* **2017**, *239* (C), 178–186 DOI: 10.1016/j.cis.2016.10.004.
- (127) Liu, X.; Haddou, M.; Grillo, I.; Mana, Z.; Chapel, J.-P.; Schatz, C. Early stage kinetics of polyelectrolyte complex coacervation monitored through stopped-flow light scattering. *Soft Matter* **2016**, 1–9 DOI: 10.1039/C6SM01979J.
- (128) Turgeon, S. L.; Beaulieu, M.; Schmitt, C.; Sanchez, C. Protein–polysaccharide interactions: phase-ordering kinetics, thermodynamic and structural aspects. *Curr. Opin. Colloid Interface Sci.* **2003**, *8*, 401–414 DOI: 10.1016/S1359-0294(03)00093-1.
- (129) Vitorazi, L.; Ould-Moussa, N.; Sekar, S.; Fresnais, J.; Loh, W.; Chapel, J. P.; Berret, J. F. Evidence of a two-step process and pathway dependency in the thermodynamics of poly(diallyldimethylammonium chloride)/poly(sodium acrylate) complexation. *Soft Matter* **2014**, *10* (47), 9496–9505 DOI: 10.1039/C4SM01461H.
- (130) Amblard, M.; Fehrentz, J.-A.; Martinez, J.; Subra, G. Methods and Protocols of Modern Solid Phase Peptide Synthesis. *Molecular Biotechnology* **2006**, *33* (3), 239–254 DOI: 10.1385/MB:33:3:239.
- (131) Chang, L.-W.; Lytle, T. K.; Radhakrishna, M.; Madinya, J. J.; Vélez, J.; Sing, C. E.; Perry, S. L. Sequence and entropy-based control of complex coacervates. *Nat Commun* **2017**, *8*, 1273 DOI: 10.1038/s41467-017-01249-1.
- (132) Pacalin, N. M.; Leon, L.; Tirrell, M. Directing the phase behavior of polyelectrolyte complexes using chiral patterned peptides. *Eur. Phys. J. Spec. Top.* **2016**, *225* (8-9), 1805–1815 DOI: 10.1140/epjst/e2016-60149-6.
- (133) Kramer, J. R.; Deming, T. J. General Method for Purification of α -Amino acid- N-carboxyanhydrides Using Flash Chromatography. *Biomacromolecules* **2010**, *11* (12), 3668–3672 DOI: 10.1021/bm101123k.
- (134) Blocher McTigue, W. C.; Perry, S. L. Incorporation of Proteins into Complex Coacervates. *Methods in Enzymology* **2020**, Submitted.
- (135) Blocher McTigue, W. C.; Perry, S. L. Design Rules for Encapsulating Proteins into Complex Coacervates. *Soft Matter* **2019**, *15*, 3089–3103 DOI: 10.1039/C9SM00372J.
- (136) Perry, S. L. Phase separation: Bridging polymer physics and biology. *Curr. Opin. Colloid Interface Sci.* **2019**, *39*, 86–97 DOI: 10.1016/j.cocis.2019.01.007.
- (137) Liu, Y.; Winter, H. H.; Perry, S. L. Linear viscoelasticity of complex coacervates. *Adv. Colloid Interface Sci.* **2017**, *239*, 46–60 DOI: 10.1016/j.cis.2016.08.010.
- (138) Rubinstein, M.; Colby, R. H. *Polymer Physics*; Oxford University Press, 2003.
- (139) Liu, Y.; Chalarca, C. F. S.; Carmean, R. N.; Olson, R. A.; Madinya, J. J.; Sumerlin, B. S.; Sing, C. E.; Emerick, T.; Perry, S. L. *Effect of Polymer Chemistry on the Linear Viscoelasticity of Complex Coacervates*; 2020; p Submitted.
- (140) Sun, J.; Perry, S. L.; Schiffman, J. D. Electrospinning Nanofibers from Chitosan/Hyaluronic Acid Complex Coacervates. *Biomacromolecules* **2019**, *20*, 4191–4198 DOI: 10.1021/acs.biomac.9b01072.

- (141) Spruijt, E.; Sprakel, J.; Lemmers, M.; Cohen Stuart, M. A.; van der Gucht, J. Relaxation Dynamics at Different Time Scales in Electrostatic Complexes: Time-Salt Superposition. *Phys. Rev. Lett.* **2010**, *105* (20), 208301–208304 DOI: 10.1103/PhysRevLett.105.208301.
- (142) Spruijt, E.; Cohen Stuart, M. A.; van der Gucht, J. Linear viscoelasticity of polyelectrolyte complex coacervates. *Macromolecules* **2013**, *46* (4), 1633–1641 DOI: 10.1021/ma301730n.
- (143) Wang, Q.; Schlenoff, J. B. The polyelectrolyte complex/coacervate continuum. *Macromolecules* **2014**, *47* (9), 3108–3116 DOI: 10.1021/ma500500q.
- (144) Schaaf, P.; Schlenoff, J. B. Saloplastics: Processing compact polyelectrolyte complexes. *Adv. Mater.* **2015**, *27* (15), 2420–2432 DOI: 10.1002/adma.201500176.
- (145) Sadman, K.; Wang, Q.; Chen, Y.; Keshavarz, B.; Jiang, Z.; Shull, K. R. Influence of Hydrophobicity on Polyelectrolyte Complexation. *Macromolecules* **2017**, *50* (23), 9417–9426 DOI: 10.1021/acs.macromol.7b02031.
- (146) Hofmeister, F. Zur Lehre von der Wirkung der Salze. *Archiv f experiment Pathol u Pharmakol* **25**, 1–30.
- (147) Zhang, Y.; Cremer, P. S. Interactions between macromolecules and ions: the Hofmeister series. *Curr. Opin. Chem. Biol.* **2006**, *10* (6), 658–663 DOI: 10.1016/j.cbpa.2006.09.020.
- (148) Kunz, W.; Nostro, Lo, P.; Ninham, B. W. The present state of affairs with Hofmeister effects. *Curr. Opin. Colloid Interface Sci.* **2004**, *9* (1-2), 1–18 DOI: 10.1016/j.cocis.2004.05.004.
- (149) Collins, K. D. Ions from the Hofmeister Series and Osmolytes: Effects on Proteins in Solution and in the Crystallization Process. *Methods* **2004**, *34* (3), 300–311 DOI: 10.1016/j.ymeth.2004.03.021.
- (150) Salis, A.; Ninham, B. W. Models and mechanisms of Hofmeister effects in electrolyte solutions, and colloid and protein systems revisited. *Chem. Soc. Rev.* **2014**, *43*, 7358–7377 DOI: 10.1039/C4CS00144C.

Table of Contents Entry



We describe a strategy that tracks the evolution of turbidity for poorly mixed samples to characterize the kinetics of coacervation.